Wave-number spectrum of electrocorticographic signals

S. C. O'Connor and P. A. Robinson
School of Physics, University of Sydney, New South Wales 2006, Australia
and Brain Dynamics Center, Westmead Hospital and University of Sydney, Westmead, New South Wales 2145, Australia
(Received 21 October 2002; published 16 May 2003)

A physiologically based continuum model of corticothalamic electrodynamics is generalized and used to derive the theoretical form of the electrocorticographic (ECoG) wave-number spectrum. A one-dimensional projection of the spectrum is derived, as is the azimuthally averaged two-dimensional spectrum for isotropic and anisotropic cortices. The predicted spectra are found to consist of a low-k plateau followed by three regions of power-law decrease, which result from filtering of the electrical activity through physical structures at different scales in the cortex. The magnitude of the maximum theoretical power-law exponent is larger for the two-dimensional (2D) spectrum than for its 1D counterpart. The predicted spectra agree well with experimental data obtained from 1D and 2D recording arrays on the cortical surface, enabling the structures in the brain that are important in determining spatial cortical dynamics to be identified. The cortical dispersion relation predicted by our model is also investigated, providing insight into the relationships between temporal and spatial brain dynamics.

DOI: 10.1103/PhysRevE.67.051912 PACS number(s): 87.10.+e, 87.18.Hf, 87.19.La

I. INTRODUCTION

The electroencephalogram (EEG) and electrocorticogram (ECoG) are recordings of brain electrical activity from electrodes on the scalp and the cortical surface respectively. These have been widely investigated in the temporal domain for a variety of brain states and disorders [1–10].

In the spatial domain, research has been mostly concentrated on topographic studies of power [11–14], the question of how the brain correlates different aspects of a single stimulus [15,16], and spatial coherence [3,17,18].

We are concerned here with the wave-number content of brain activity, which has received relatively little attention despite its potential to provide insight into brain function from a new perspective. Some authors have recorded the wave-number content of activity in the brain, both from electrodes on the scalp [19–21] and from electrodes on the cortical surface [22–24]. The former have been shown to give good agreement with a scalp wave-number spectrum which was theoretically derived using a neurophysical continuum model of cortical dynamics [25].

Here we extend the above model to analyze the wave-number spectrum on the cortical surface, which is particularly useful for investigation of the small scales that are not accessible from the relatively coarsely resolved scalp spectra. Derivation of the wave-number spectrum represents one application of the model, which is also able to reproduce many of the temporal characteristics of the EEG, such as the spectral peaks [26–28], evoked response potentials (ERPs) [28], trends seen in various states of arousal [29], and certain seizure onsets and dynamics [30]. It has also addressed modal effects arising from cortical boundary conditions [27], and spatial coherence and correlations [31]. In the reverse direction, an individual's frequency power spectrum can be fitted to the model and the underlying physiological parameters thereby deduced [30,32].

Second, we investigate the cortical dispersion relation as it arises in our model. The existence of a dispersion relation for waves in the brain was postulated decades ago [33–35] and has since been studied by various authors [21,36,37]. We investigate it within the context of our model with an aim of shedding light on both its detailed structure and how it interrelates the temporal and spatial components of brain activity.

Third, we compare the predicted cortical spectra with data obtained from two ECoG experiments [23,24]. We restrict our comparison to data taken from neocortical arrays, since the olfactory bulb and paleocortex which feature in some experiments [22,24] have different anatomical structure and exhibit some different behaviors [13] from the neocortex upon which the cortical part of our model is based.

In Sec. II of this paper our model is briefly outlined. A brief discussion of the spatial scales in the brain follows in Sec. III. The resulting considerations are included in the model in Sec. IV, where the spatial spectra are derived for both the two-dimensional (2D) case and its projection onto one dimension. In Sec. V the features of the predicted spectra are investigated analytically, and the dispersion relation is discussed. The predictions are compared with experiment in Sec. VI for both the 1D and 2D spectra.

II. CORTICOTHALAMIC MODEL

In this section, we summarize the corticothalamic model developed previously. The cortex is modeled as a 2D sheet, which is motivated by its relative thinness. Cortical boundary conditions are neglected, thus the cortex is effectively modeled as an infinite sheet, an approximation which has yielded good agreement with observed spectra using this model [27]. The implications of neglecting boundary conditions are discussed more fully in Sec. III.

The model assumes randomly interconnected excitatory and inhibitory neurons. Scales below a few tenths of a millimeter are averaged over to yield a continuum treatment that extends from this scale to that of the whole cortex, as in similar models [21,38–41]. Thus, the firing rates of signals emitted by single excitatory e or inhibitory i neurons, which

depend on their individual cell-body potentials, are averaged to give local mean values of the outgoing pulse field $\phi_a, a = e, i$. The propagating pulse field density ϕ_a is then proportional to measured large-scale potentials, such as the ECoG.

The mean rate of generation of neuronal pulse density has a sigmoidal dependence on the mean local cell-body potential, which we approximate here by a linear function on the assumption that deviations from the steady state are small at large scales in normal, nonseizure states. This approximation has been found to yield excellent agreement with observed frequency spectra [29].

The local mean cell-body potential V_a of neurons of type a in the cortex is a function of inputs from other cortical neurons, and from excitatory subcortical neurons. Incoming activity is received in the dendritic tree and filtered as it travels along the dendrites to the cell-body. Thus, the cell-body potential of a neuron of type $a = e, i$ can be written in Fourier space as

$$V_a(\mathbf{k},\omega) = \sum_b L_a(\omega) G_{ab} \phi_b(\mathbf{k},\omega), \tag{1}$$

where $b = e, i, s$ and the G_{ab} are dimensionless gains representing the response strength in neurons a due to a unit signal incident from neurons of type b. The quantity L_a is a dendritic low-pass filter function which accounts for the temporal delay and smearing of the incoming signal as it travels along the dendritic tree to the cell-body. It can be written [42] as

$$L_a(\omega) = (1 - i\omega/\alpha)^{-1}(1 - i\omega/\beta)^{-1}, \tag{2}$$

where β and α are inverse rise and decay times of the dendritic potential, respectively.

Outgoing pulses from each neuron propagate along its axonal tree at a velocity $v \approx 10\ \mathrm{m\,s^{-1}}$. This propagation can be described by damped wave equations for the fields ϕ_a [42]. In Fourier space one finds

$$D_a(\mathbf{k},\omega)\phi_a(\mathbf{k},\omega) = V_a(\mathbf{k},\omega), \tag{3}$$

where

$$D_a(\mathbf{k},\omega) = k^2 r_a^2 + (1 - i\omega/\gamma_a)^2, \tag{4}$$

$\gamma_a = v/r_a$ is a measure of the damping, and r_a is the mean range of axons a.

Most subcortical signals ϕ_s arrive at the cortex from the relay nuclei of the thalamus. The thalamocortical connectivity assumed in the model is shown in Fig. 1, involving the cortex, the thalamic relay nuclei, and the thalamic reticular nucleus. The (roughly 15) relay nuclei convey sensory information to relevant areas of the cortex [43]. These nuclei also receive signals from the cortex which they topographically feed back to it. The thalamic reticular nucleus receives excitatory inputs from both thalamic relay and cortical neurons. Its output is inhibitory and acts solely on relay nuclei.

With reference to Fig. 1, we see that subcortical input ϕ_s to the cortex is a filtered combination of subthalamic inputs ϕ_n and a feedback signal originating from ϕ_e in the cortex.

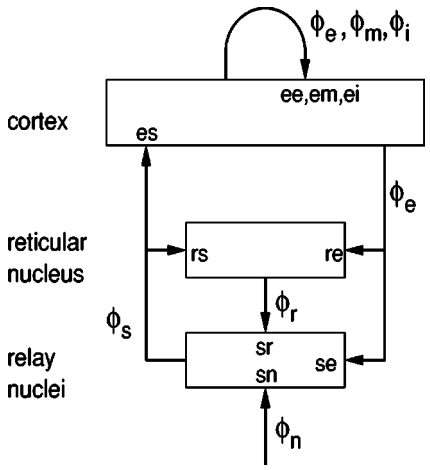

FIG. 1. Diagram of corticothalamic connections showing the cortex, reticular nucleus, and relay nuclei. The cortex is extensively connected to itself, and also projects to and receives projections from the thalamus. There are two loops through the thalamus: a direct loop passing only through the relay nuclei, and an indirect loop which also passes through the reticular nucleus. There is also an intrathalamic loop. Corticothalamic gains are indicated on the diagram.

If the time taken for a signal to travel from the cortex through the thalamus and back is t_0, we can write [28]

$$\phi_s(\mathbf{k},\omega) = P(\omega)\phi_n(\mathbf{k},\omega) + S(\omega)\phi_e(\mathbf{k},\omega), \tag{5}$$

where

$$P(\omega) = \frac{L_s G_{sn}}{1 - L_s G_{sr} L_r G_{rs}} e^{i\omega t_0/2}, \tag{6}$$

$$S(\omega) = \frac{L_s G_{sr} L_r G_{re} + L_s G_{se}}{1 - L_s G_{sr} L_r G_{rs}} e^{i\omega t_0}, \tag{7}$$

and ϕ_n is approximated as spatiotemporal white noise.

Incorporation of Eqs. (5)–(7) into Eq. (1), followed by elimination of V_a from Eq. (1) and (3), yields the transfer functions [28]

$$\frac{\phi_e(\mathbf{k},\omega)}{\phi_n(\mathbf{k},\omega)} = \frac{L_e G_{es} P}{1 - L_i G_{ii}} \frac{1}{k^2 r_e^2 + q^2 r_e^2}, \tag{8}$$

$$\frac{\phi_i(\mathbf{k},\omega)}{\phi_n(\mathbf{k},\omega)} = \frac{D_e L_i G_{is}}{D_i L_e G_{es}} \frac{\phi_e}{\phi_n}, \tag{9}$$

where

$$q^2 r_e^2 = (1 - i\omega/\gamma_e)^2 - \frac{L_e G_{ee} + L_e G_{es} S}{1 - L_i G_{ii}}. \tag{10}$$

III. SCALES IN THE CORTEX

In this section we discuss the structures in the cortex which could contribute to spatial filtering at various scales, and hence deduce that an additional population of neurons should be introduced into our model with characteristic

range of a few millimeters, which is the approximate length of recurrent collaterals, the local axons which emanate from otherwise long-range excitatory pyramidal neurons.

At global scales, the physical size of the cortex affects the dynamics. As such, we would expect the boundary conditions to play a role in determining the form of both wave-number and frequency spectra for very small **k**. The extent of their influence on the dynamics of this model has been investigated in previous work [27] and the parameter, wave-number, and frequency regimes in which their effects are significant have been identified, which correspond to where damping is the weakest. It was concluded that, for most realistic parameters, detailed boundary conditions are not very important in determining the form of the power spectrum produced by this model, in contrast to some other models in which boundary conditions play a more critical role in determing dynamics because damping is intrinsically weak [21]. In our model, we have shown empirically that under most circumstances boundary conditions may be ignored [27]. We therefore model the cortex as infinite in the present work. Note that in any case the wave-number range corresponding to the ECoG is well above the global scale, so the comparisons with the ECoG experiments in Sec. VI should be unaffected by cortical boundary conditions. For smaller brains, such as the rabbit brain, boundary conditions might have a greater influence on dynamics, probably enhancing spectral power at low frequencies [27]. At the large wave numbers corresponding to the ECoG, however, these effects should be minimal.

Below global scales, there are structures such as prominent sulci (the ''grooves'' visible when the brain is viewed as a whole) and gyri (located between the sulci), and their associated lobes. The details of the convolutions are expected to have minimal effects on the cortical dynamics [21,27], even considering the fact that long-range axons can cut across fissures [21], because of the relative insensitivity of the model to boundary conditions. As such, the details of the cortical convolutions are ignored in the present study, however, the increase in effective cortical size as a result of the folding is incorporated by inclusion of a cortical folding parameter.

The ranges of excitatory connections vary from short to long scale and can reach ≈ 40 cm in length, following a distribution with an exponential fall off peaked at $r_e = 5-10$ cm [21,44]. These filter out the excitatory component of the observed cortical power above $k \approx 1/r_e$ [25], and are included in our model. Shorter-scale inhibitory connections of average range $r_i \approx 0.1$ mm are also included in our model. These filter out the remaining inhibitory power above $k \approx 1/r_i$.

Excitatory and inhibitory neurons, however, are each also associated with two other scales that are not included in the model. These are the width of the arborization column of incoming (afferent) signals, and the extent of their outgoing (efferent) collateral systems; that is, their input and output scales. For inhibitory neurons, the input and output scales are both well below the range of validity of the continuum approximations made in the model (a few tenths of a millimeter and above), and any detail at these lengths is averaged over. For excitatory neurons, however, this is not the case.

Incoming excitatory signals do not target a single cortical neuron, but extend over a region ≈ 0.3 mm in diameter [21]. This input scale of excitatory neurons is sometimes referred to as a cortical column [21]. An excitatory population at this scale has been included in our model in previous work [28] where it was shown to be indistinguishable in practice from the inhibitory population except for sign, with the net effect depending only on the weighted sum. For simplicity of nomenclature we denote the net effect of the two populations with a single subscript *i* and refer to it as inhibitory, but note here that it includes the dynamics of any excitatory neural population with mean axonal range $\lesssim 0.3$ mm.

We now consider the output scale of excitatory neurons. This refers to the fact that a given excitatory neuron does not project only to distant regions in the brain, but has a number of recurrent collaterals which output locally. They are typically thought to extend over a couple of millimeters [21], though work on the monkey cortex has found collateral systems which exceed 6 mm [45,46]. This scale is often termed a macrocolumn [21], and is not included in the above version of our model. We include it here and gauge its effect on the spatial spectrum.

The details of structures at smaller scales than those discussed above are well outside the scope of this model, which averages over all details at scales below a few tenths of a millimeter. Such structures include not only the input and output ranges of inhibitory neurons, but all other cellular details such as the size of individual cells, axon, and dendrite diameters, etc.

IV. GENERALIZED MODEL

In this section, we include the excitatory recurrent collaterals by introducing a second excitatory population with a range of a few millimeters. We use the resulting transfer functions to derive the form of the wave-number spectrum on the cortical surface for both the full 2D wave vector spectrum and its 1D projection.

We denote the additional population with the subscript *m*. The derivation of the new model equations follows that of Rennie *et al.* [28] who also included a third neuron population, although different in detail.

The transfer equations for the three populations are

$$\frac{\phi_e(\mathbf{k},\omega)}{\phi_n(\mathbf{k},\omega)} = \frac{L_e G_{es} P \lambda M}{k^2 r_e^2 + q_e^2 r_e^2}, \tag{11}$$

$$\frac{\phi_m(\mathbf{k},\omega)}{\phi_n(\mathbf{k},\omega)} = \frac{D_e L_m G_{ms}}{D_m L_e G_{es}} \frac{\phi_e}{\phi_n}, \tag{12}$$

$$\frac{\phi_i(\mathbf{k},\omega)}{\phi_n(\mathbf{k},\omega)} = \frac{D_e L_i G_{is}}{D_i L_e G_{es}} \frac{\phi_e}{\phi_n}, \tag{13}$$

where

$$\lambda = \frac{1}{1 - L_i G_{ii} - L_m G_{mm}}, \tag{14}$$

$$q^2 r_e^2 = (1 - i\omega/\gamma_e)^2 - \lambda(L_e G_{ee} + L_e G_{es} S), \tag{15}$$

$$M = \frac{D_e L_m G_{mm} D_i (1 - D_m) + D_e D_m L_i G_{ii} (1 - D_i)}{\det} + 1, \tag{16}$$

$$\det = D_e D_m D_i - (L_e G_{ee} + L_e G_{es} S) D_m D_i - D_e D_i L_m G_{mm} - D_e D_m L_i G_{ii}. \tag{17}$$

Note that the axon length r_i is sufficiently small that $D_i \approx 1$, which allowed the approximation $M = 1$ to be made in previous work on the wave-number spectrum using this model [25]. In the present work, the spatial extent of recurrent collaterals r_m is too large to justify this approximation.

A. 1D spectrum

The 1D projected spectrum on the cortical surface is given by

$$P_a(k_x, \omega) = \int_{-\infty}^{\infty} |\phi_a(\mathbf{k}, \omega)|^2 dk_y, \tag{18}$$

for each of the populations $a = e, m, i$. The observable potential is a linear combination of each of these populations, which also gives rise to cross terms which are discussed in Sec. IV C. In the limit $M = 1$, previous work [25] has shown that for the excitatory and inhibitory populations, the cortical power has the form

$$P_e(k_x, \omega) = A_e \int_{-\infty}^{\infty} \frac{dk_y}{|k^2 + q_e^2|^2}, \tag{19}$$

$$P_i(k_x, \omega) = \int_{-\infty}^{\infty} \frac{A_{i1} k_y^4 + A_{i2} k_y^2 + A_{i3}}{|k^2 + q_i^2|^2 |k^2 + q_e^2|^2} dk_y, \tag{20}$$

where

$$q_i = (1 - i\omega/\gamma_i)/r_i \tag{21}$$

and the A_a depend on ω and k_x but are constants of the integration. Similarly for the m population,

$$P_m(k_x, \omega) = \int_{-\infty}^{\infty} \frac{A_{m1} k_y^4 + A_{m2} k_y^2 + A_{m3}}{|k^2 + q_m^2|^2 |k^2 + q_e^2|^2} dk_y, \tag{22}$$

where

$$q_m = (1 - i\omega/\gamma_m)/r_m. \tag{23}$$

Thus, to a first approximation, we can write for $a = e, m, i$,

$$|q_a| \approx 1/r_a, \tag{24}$$

which represents the onset of spatial filtering due to the a neural population. For long-range excitatory power, this can be seen qualitatively from Eq. (19), where for $k < |q_e|$ the power spectrum is flat, and for $k > |q_e|$ it is of the form k^{-g} with g approximately constant. Similar reasoning applies to the m and i spectra. We henceforth refer to $k_x \approx |q_e|, k_x \approx |q_m|$, and $k_x \approx |q_i|$ as the e, m, and i knees, respectively, since they manifest themselves as knees in the spectrum.

The inclusion here of $M \neq 1$ does not affect these approximate relationships which determine the general form of the wave-number spectrum [25], but alters its detailed shape. We note here simply that the spatial component of M depends only on the D_a, which in turn depend on axonal ranges r_a. The quantity M differs significantly from unity only at wave numbers above $\approx q_m$, so we expect M to have little effect on the cortical spectrum for wave numbers below $|q_m|$, and greatest effect at the m and i knees where M changes relatively quickly.

For our purposes, sufficient qualitative analytic insight into the spectral structure can be obtained from Eqs. (19), (20), and (22), so the integrals are not calculated explicitly here, but are evaluated numerically in what follows. For explicit analytical results of similar integrals, see Ref. [25].

B. Azimuthally averaged 2D spectrum

We calculate the full 2D wave-number spectrum to allow comparison with data obtained from 2D electrode arrays on the cortex. The simple case of an isotropic cortex in which activity is independent of direction is considered first, followed by the more general and realistic anisotropic case in which a typical length scale in the anterioposterior direction (front to back) differs from that in the mediolateral direction (left to right) [47,48]. In both cases, the power at a given wave-number is integrated over all directions, giving a spectrum that can be presented as a function of $k = |\mathbf{k}|$. This facilitates comparison in Sec. VI B with experimental data collected by Barrie *et al.* [24], which is summed in the same way.

For an isotropic cortex the transfer functions (11)–(13) have no angular dependence, so integrating over direction simply introduces a factor of 2π. Therefore, the power in the three populations is given by

$$P_e(k, \omega) = \frac{2\pi |L_e G_{es} P \phi_n M \lambda|^2}{r_e^4 |k^2 + q_e^2|^2}, \tag{25}$$

$$P_m(k, \omega) = \frac{2\pi |L_m G_{ms} P \phi_n M \lambda D_e|^2}{r_e^4 r_m^4 |k^2 + q_e^2|^2 |k^2 + q_m^2|^2}, \tag{26}$$

$$P_i(k, \omega) = \frac{2\pi |L_i G_{is} P \phi_n M \lambda D_e|^2}{r_e^4 r_i^4 |k^2 + q_e^2|^2 |k^2 + q_i^2|^2}. \tag{27}$$

The denominators give the wave numbers that correspond to the onset of spatial filtering due to each of the populations, as approximated by Eq. (24).

For an anisotropic cortex we convert to polar coordinates and introduce an elliptical anisotropy whereby r_a^2 is replaced as follows:

$$r_a^2 \Rightarrow \frac{2 r_a^2 (\cos^2\theta + b^2 \sin^2\theta)}{(1 + b^2)}, \tag{28}$$

where $b=1$ corresponds to the isotropic case, and typically $b\approx 2$ in the cortex [47,48]. Note that the mean $\langle r_a^2\rangle$ is unchanged by this replacement. Making this substitution, we have

$$P_e(k,\omega)=A_e\int_0^{2\pi}\frac{|M|^2|\cos^2\theta+b^2\sin^2\theta|^{-2}}{|k^2+q_e^2|^2}d\theta, \quad (29)$$

$$P_m(k,\omega)=A_m\int_0^{2\pi}\frac{|MD_e|^2|\cos^2\theta+b^2\sin^2\theta|^{-4}}{|k^2+q_e^2|^2|k^2+q_m^2|^2}d\theta, \quad (30)$$

$$P_i(k,\omega)=A_i\int_0^{2\pi}\frac{|MD_e|^2|\cos^2\theta+b^2\sin^2\theta|^{-4}}{|k^2+q_e^2|^2|k^2+q_i^2|^2}d\theta, \quad (31)$$

where $M(\theta)$ is as given in Eq. (16) but with

$$D_a(\omega)=\frac{2k^2r_a^2}{1+b^2}(\cos^2\theta+b^2\sin^2\theta)+(1-i\omega/\gamma_a)^2. \quad (32)$$

C. Cross terms

As mentioned earlier, the experimentally measured potential is a linear combination of the fields of the three neuron populations [28]. The measured power for the 1D spectrum, for example, is then given by

$$P(k_x,\omega)=\int_{-\infty}^{\infty}|W_e\phi_e+W_m\phi_m+W_i\phi_i|^2dk_y \quad (33)$$

$$=W_e^2P_e+W_m^2P_m+W_i^2P_i+2W_eW_mP_{em}+2W_eW_iP_{ei}+2W_mW_iP_{mi}, \quad (34)$$

where the W_a represent the relative numbers of each type of neuron in the cortex, weighted by structural and orientation factors that affect their ability to generate observable potentials [28]. The W_a are assumed here to be independent of ω and $\mathbf{k}$. The quantities P_e, P_m, and P_i are derived above, and the quantities P_{em}, P_{ei}, and P_{mi} are incorporated numerically into formulation of the cortical power spectra using

$$P_{ab}(k_x,\omega)=\mathrm{Re}\int_{-\infty}^{\infty}\phi_a(\mathbf{k},\omega)\phi_b^*(\mathbf{k},\omega)dk_y, \quad (35)$$

for $a,b=e,m,i$. For 2D spectra the analogous equation is

$$P_{ab}(k,\omega)=\mathrm{Re}\int_{-\infty}^{\infty}\phi_a(k,\theta,\omega)\phi_b^*(k,\theta,\omega)d\theta. \quad (36)$$

D. Constraints on the midrange population

We have introduced a second excitatory neuron population, thereby increasing the number of parameters in the model. In particular, we have introduced the quantities r_m and W_m which, respectively, describe the mean range and weighted contribution to the observable power of the new population. We now summarize the constraints on these quantities imposed by physiological and anatomical considerations of the recurrent collateral system.

The range of excitatory recurrent collaterals in humans varies from 0.5 mm to 3 mm [21], though collaterals in monkeys have been found up to 6 mm to 10 mm in length [45,46]. We therefore require that $r_m\gtrsim 0.5$ mm in all of our modeling, and approximate the mean range by $r_m=2$ mm, noting that ranges greater than 6 mm are consistent with physiology.

The relative contribution of the midrange *m* population is affected by both cortical connectivity, and orientation and structural factors which affect the neuron's ability to generate observable potentials. These quantities are not well quantified in the literature, however, the probability that a neuron synapses on a nearby neuron is $\approx 10\%$ [49], thus we expect the weighting of the *m* population to be $\approx 10\%$ of that of the *e* population. This figure is not adjusted for structural factors since both populations emanate from the same (pyramidal) neurons. Inhibitory *i* neurons, however, contribute much less to the observable power due to their lower prevalence, their structure, and their nonaligned orientation [25,50]. We therefore set $W_m=0.1W_e$ in all our modeling, and take $W_e+W_m+W_i=1$ without loss of generality. Here, we make the approximation $W_e\approx 0.9$, as listed in Table I, which is consistent with physiological, anatomical, and other modeling studies [21,25,50].

V. THEORETICAL PREDICTIONS

In this section, we study the predicted theoretical cortical wave-number spectra. We analyze both the projected 1D spectrum and the full 2D spectrum, and discuss their frequency dependence via a cortical dispersion relation. The model parameters used to generate the spectra in each case are given in Table I. Wherever possible, these are taken directly from experiment, although more often only physiologically realistic ranges can be deduced, which can easily span a factor of 2. In such cases, the parameters are estimated from extensive comparisons and fitting of the model to experiment, and always lie within the physiologically realistic ranges. The estimated parameters for a given brain state accurately reproduce data from a wide variety of experiments, including both spatial and temporal EEGs and ERPs, with only modest variations in their values, and are always consistent with known physiological constraints. Furthermore, within our model, significantly different combinations of parameters do not produce results that are consistent with experiment. This lends confidence that if the theory accurately models brain dynamics, the actual parameters in the brain are close to those given in Table I. For a more extensive discussion of the model parameters and their applicability to genuine brains for a variety of brain states, see Refs. [30,32].

A. 1D projected spectrum

The predicted 1D spectrum given by Eq. (34) is shown in Fig. 2. The solid curve represents the observable power $P(k_x,\omega)$, the dashed curves represent the power due to each of the three populations P_e, P_m, and P_i, and the dotted

TABLE I. Parameters used in the model. The second and third columns give human parameters, and the fourth gives rabbit parameters. The human parameters were chosen based on both physiological considerations and previous work using this model, and values of the new independent parameter r_m and the weightings W_a are discussed in Sec. IV D. The rabbit parameters were adapted from human parameters for the awake eyes-open state based on physiological and anatomical considerations, as discussed in Sec. V B.

Parameter	Anesthesia	Eyes closed	Rabbit	Unit
t_0	0.08	0.08	0.015	s
r_e	80	80	15	mm
r_m	2	2	1.4	mm
r_i	0.05	0.05	0.05	mm
γ_e	100	100	250	s^{-1}
γ_m	3000	3000	2000	s^{-1}
γ_i	10^5	10^5	5×10^4	s^{-1}
$\alpha=\beta/4$	50	120	75	s^{-1}
$G_{es}=G_{ms}=G_{is}$	1.3	3.9	5.0	
G_{se}	0.3	2.6	1.0	
G_{sr}	-0.2	-3.0	-1.0	
G_{rs}	2.6	0.6	-0.1	
$G_{ee}=G_{mm}$	1.0	6.2	4.0	
G_{ii}	-1.9	-10	-2.3	
G_{re}	4.0	0.3	0.5	
G_{sn}	7.0	5.0	3.0	
W_e	0.9	0.9	0.9	

curves represent the power due to the cross terms, P_{em}, P_{ei}, and P_{mi}. The model parameters used to generate this spectrum are given in Table I under the heading "anesthesia," and are very similar to those used by this model to generate temporal power spectra, ERPs, and scalp wave-number spectra [25,28,30,32].

The observable spectrum has a plateau in power at low wave numbers, followed by three regions of power-law decrease, each separated by an incompletely developed plateau. This is similar to the theoretical EEG spectrum produced by this model [25] which has a low-k_x plateau followed by two regions of power-law decrease. The third power-law decrease

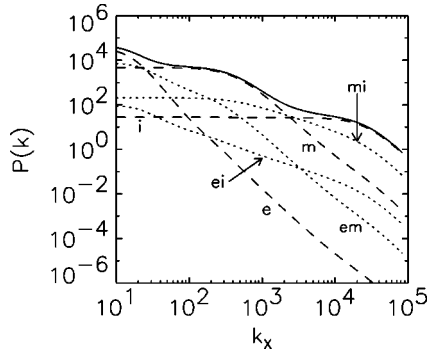

FIG. 2. One-dimensional wave-number power spectrum from Eq. (34) derived from the model (solid line), integrated over 5 Hz $\leqslant f \leqslant$ 50 Hz. Also shown are the weighted power contributions from each of the neuron populations $2W_e^2P_e$, $2W_m^2P_m$, and $2W_i^2P_i$ (dashed lines), and their weighted interference power contributions (dotted lines). Parameters are for human brains under anesthesia, given in Table I.

region in the present work is due to the introduction of the midrange *m* population. A further difference between the cortical spectrum presented here and the scalp spectrum [25] is the lack of filtering due to volume conduction through the head in the present case.

In order to better understand the spectrum, we examine each of the contributing curves individually. Consider first the power contributions P_e, P_m, and P_i, from each neuron population (dashed curves in Fig. 2). Each of these has a low-k_x plateau followed by a power-law decrease, with the transitional knee between the two behaviors occurring at the wave numbers given by Eq. (24) for P_e, P_m, and P_i, respectively, similarly to the scalp spectrum [25]. We have shown previously that the slope of the high-k_x power-law region in each case is -3 in the limit $M=1$ [25]. The effect of nonunity M is slight kinks in the curves at $k_x \approx 10^3\ \mathrm{m}^{-1} \approx 1/r_m$ and $k_x \approx 10^4\ \mathrm{m}^{-1} \approx 1/r_i$. Note that these kinks are not obvious for the parameters used to generate Fig. 2.

Consider now the interference power contributions (dotted curves in Fig. 2). These are intermediate in character between the two interfering populations, for example, P_{ei} has a knee at both $|q_e|$ and $|q_i|$, with a slope varying from 0 at $k_x < |q_e|$ to -3 at $k_x > |q_i|$. Similarly, P_{em} and P_{mi} each has two knees and reaches a maximum slope of -3 at large k_x.

The observable spectrum is simply the sum of the individual curves considered above. Thus, we find that the observable spectral power decreases with wave-number according to the power law

$$P(k_x,\omega) \propto k_x^{-g}, \tag{37}$$

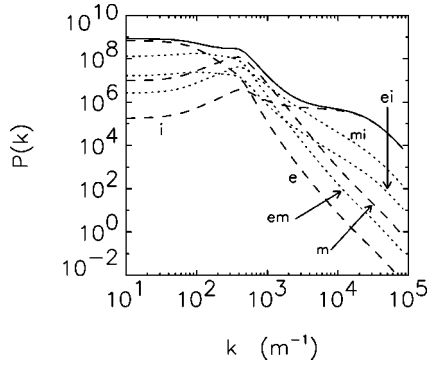

FIG. 3. Two-dimensional isotropic wave-number power spectrum from Eq. (34) derived from the model (solid line), integrated over 5 Hz $\leqslant f \leqslant$ 100 Hz. Also shown are the weighted power contributions from each of the neuron populations $2W_e^2P_e$, $2W_m^2P_m$, and $2W_i^2P_i$ (dashed lines), and their weighted interference power contributions (dotted lines). Parameters are for awake rabbit brains, given in Table I.

where the exponent g varies within the range $0 \leqslant g \leqslant 3$. The exact value of g at each point of the spectrum depends on the model parameters, but must lie within this range. This result for the cortical spectrum is the same as that for the scalp spectrum [25], except for the fact that in the scalp spectrum wave numbers above $k_0 \approx 25\ \mathrm{m}^{-1}$ are additionally filtered by volume conduction of the signal as it passes through the head, giving a greater maximum value of the exponent g.

B. Azimuthally averaged 2D spectrum

We first investigate the isotropic 2D spectrum, then turn our attention to the more general anisotropic case. The isotropic 2D spectrum predicted by the model is shown in Fig. 3. The solid line represents the observable spectrum, the dashed lines represent the power due to each of the three neuron populations, and the dotted lines represent the power due to the cross terms. The parameters used to generate this spectrum are given in Table I, for rabbits. The model was primarily developed to provide insight into the human brain, however, the lack of suitable published human 2D ECoG data has necessitated the use of comparison with the available rabbit data. We now explore the theoretical spectrum, and in Sec. IV compare the predictions with rabbit data.

Data were recorded from awake rabbits with open eyes, hence we adapt human eyes-open parameters which were chosen based on both physiological considerations and previous work using this model [25] as discussed above. The scale parameters, which are the most affected by the change, are shown above the line in Table I. The long-range parameter r_e is reduced from the human value by a factor ≈ 5, the ratio of linear scale sizes for rabbit and human brains [21]. The shorter-scale ranges are increasingly less affected by the reduction in brain size, and so are reduced by increasingly smaller amounts. The mean conduction velocity in rabbit axons is reduced from the human value to $v \approx 5\ \mathrm{m\,s}^{-1}$ [51,52], which combined with the decrease in spatial ranges r_a leads to a change in the damping parameters according to $\gamma_a = v/r_a$.

Parameters below the line are not directly related to brain size, and so are left unchanged from their human values. The one exception is the thalamocortical input G_{as} which has been increased from the human eyes-open value by a factor of 5 to reflect the fact that the ratio of midbrain to cortico-cortical inputs is higher in rabbits than in humans by approximately this factor [21,53]. Note that the human spectrum is easily obtained by using appropriate parameters, and does not differ qualitatively from the rabbit spectrum.

Let us now consider Fig. 3. The spectrum is similar to the 1D spectrum in that it consists of a low-k_x plateau followed by regions of power-law decrease due to the finite range of each of the neuron populations. The most striking difference is the large hump in the m and i power curves beginning at $k_x \approx 1/r_e$. We investigate this further by studying the individual power curves separately. We begin by exploring the curves in the limit $M=1$, and later infer the effect of $M \neq 1$.

A cursory inspection of Eq. (25) reveals that in the limit $M=1$ the isotropic P_e spectrum decays as k^{-4} for large k, with a plateau below the knee at $k \approx 1/r_e$. For the P_m spectrum in the limit $M=1$, there is also a low-k plateau owing to the fact that the k-dependent terms $|D_e|^2, 1/|k^2+q_e^2|^2$, and $1/|k^2+q_m^2|^2$ in Eq. (26) all plateau at low wave numbers. The first two of these three terms change from plateaus to fourth-order power-law regions at a knee given approximately by $1/r_e$, though the first increases and the second decreases, thereby approximately negating one another's effects for most parameters. There are, however, certain parameters for which the terms fail to entirely negate one another. This occurs when the knees do not exactly coincide. The knees of the first and second terms occur at $1/r_e$ to a first approximation, but differ due to the second term on the right hand side of Eq. (15), and are given, respectively, by

$$k_1 = |\sqrt{\omega^2/\gamma_e^2 - 1}|/r_e, \tag{38}$$

$$k_2 = |\sqrt{\omega^2/\gamma_e^2 - 1 + a}|/r_e, \tag{39}$$

where a is the real part of the second term on the right hand side of Eq. (15). For most parameters $a \approx 0$ and the knees coincide, especially for $f \gtrsim$ 20-30 Hz. For $a \neq 0$, we would expect either a dip or a hump in the spectrum, depending on the sign of a, due to the different onsets of power-law behavior. It turns out that k_2 never falls far below k_1, but for certain gain parameters it becomes significantly larger than k_1 thereby producing a hump, and is particularly sensitive to changes in intracortical gain G_{ee}. Thus the effect of the first two of the three wave-number-dependent terms is a plateau for all k with a possible hump at around $1/r_e$ for certain parameters. The third term $1/|k^2+q_m^2|^2$ has a plateau for $k \lesssim 1/r_m$, and decreases as k^{-4} above this. Thus, the midrange excitatory spectrum P_m has a low-k plateau that turns downward at a knee at $1/r_m$ and decays thenceforth as k^{-4}, with an additional hump beginning at $k_x \approx 1/r_e$ for some gain parameters. For the rabbit parameters given in Table I there is such a hump, due to the different onsets of power-law behavior.

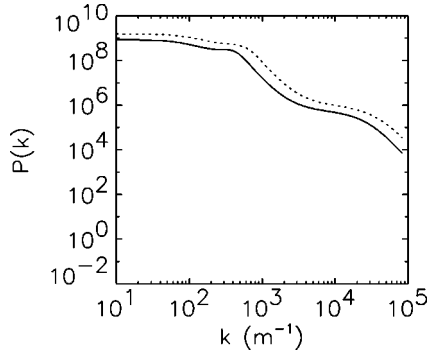

FIG. 4. Two-dimensional wave-number spectrum, parameters for awake rabbit brains, given in Table I. The anisotropic spectrum (dotted line) is slightly shifted relative to the isotropic spectrum (solid line).

Similar comments apply to the P_i inhibitory spectrum and hence the cross spectra, for $M=1$. The contribution of nonunit M is minimal, and similar to that of the 1D case. Namely, it can contribute to the kinks at $1/r_m$ and $1/r_i$. This effect is increased somewhat for certain model parameters, such as large G_{ee} and large α, as discussed in Sec. V C.

Thus the isotropic 2D spectrum takes the form of a power law given by Eq. (37) where the exponent g varies within the range $0 \leqslant g \leqslant 4$ for all of parameter space, except for possible kinks at $k=1/r_a$.

We now consider the effect of introducing the angular anisotropy (28), shown in Fig. 4. The solid line gives the isotropic spectrum discussed in relation to Fig. 3, and the broken line gives the anisotropic spectrum with $b=2$ in Eq. (28). The only effects on the spectrum are an increase in overall power and slight shifts of the three knees. The former effect is due to factors of the form $|1+b^2|/|\cos^2\theta + b^2\sin^2\theta|$, the integrals of which are greater for $b \neq 1$ than for the isotropic case $b=1$. Consequently, the appearance of these k-independent factors in Eqs. (29)–(31) results in an increase in power. The latter effect is due to the spreading of neuron ranges over $\sqrt{2/(b^2+1)}r_a$ to $\sqrt{2b^2/(b^2+1)}r_a$, which smooths and shifts the knees.

Thus, angular anisotropy shifts the spectrum without strongly affecting its shape.

C. Dispersion relation

We have shown above that both the 1D and 2D spectra can be represented as power laws with exponent g, where g depends on the model parameters but in general must lie within the ranges $0 \leqslant g \leqslant 3$ and $0 \leqslant g \leqslant 4$ for the 1D and 2D spectra, respectively. We would expect the spectra and g to also depend on temporal frequency in some **k** and ω ranges due to the existence of a cortical dispersion relation [21,25]. We now investigate this dispersion relation as it is predicted from our model. We first study the kernel function

$$K_e = \frac{1}{|k^2+q_e^2|^2}, \tag{40}$$

upon which power spectra strongly depend, and then turn our attention to other frequency-dependent factors which influence the wave-number spectrum.

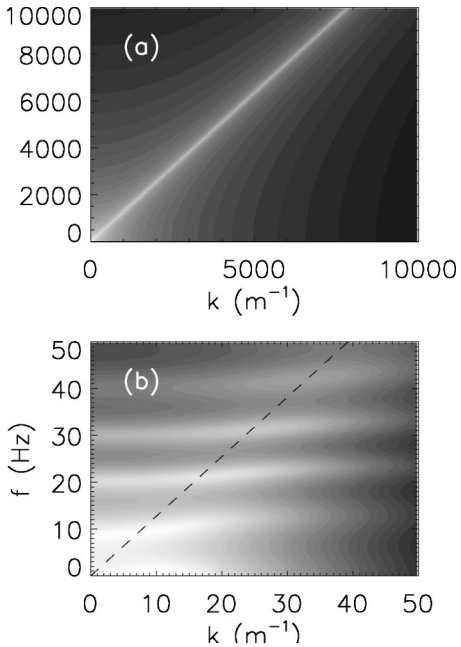

FIG. 5. The kernel function $K_e = 1/|k^2+q_e^2|^2$ as a function of wave number and frequency. Panel (a) covers the approximate wave-number range over which the model is valid and shows strong structure along the line $\omega = kv$. Panel (b) shows greater detail at low spatial and temporal frequencies, with maxima at frequencies corresponding to alpha and other resonant rhythms. The gray scale is logarithmic and its full range of shades spans 12 orders of magnitude in the upper panel and (for clarity) three orders of magnitude in the lower panel, both with the same maximum brightness.

The kernel K_e is shown in Fig. 5 as a function of frequency and wave-number for model parameters corresponding to the eyes-closed condition, as given in Table I. Figure 5(a) shows the function over the approximate wave-number range for which our continuum approach is valid. There is a striking correlation between frequency and wave number along the line $\omega = kv$ at high k and ω. This correlation can be derived from the dispersion relation obtained by setting the denominator of Eq. (11) to zero, i.e.,

$$k^2 r_e^2 + q_e^2 r_e^2 = 0. \tag{41}$$

At high ω the dendritic filter function L approaches zero, giving

$$q_e^2 r_e^2 = (1 - i\omega/\gamma_e)^2, \tag{42}$$

which we substitute into Eq. (41) to give

$$\omega = \pm kv(1 \mp i/kr_e), \tag{43}$$

and at high k

$$\omega \approx \pm kv, \tag{44}$$

to leading order in k.

Figure 5(b) shows that there is little structure apart from at low k and ω. Here we see strong structure at the alpha frequency ≈ 10 Hz, and weaker structures at its harmonics in the beta and gamma frequency ranges, reflecting the dominant signals seen in waking, eyes-closed EEG. There is also strong structure below 2 Hz, the delta frequency range that also features in recorded brain activity. Along the abscissa, there is strong structure for wave numbers below ≈ 25 m^{-1}, with diminishing strength at higher wave numbers. The function $\omega = kv$ is shown as a dashed line.

The temporal frequency power spectrum is obtained by integrating the kernel function K_e over wave number, and the excitatory wave-number power spectrum is obtained by integrating it over frequency. By examining Fig. 5(b) we can see that the structures predicted by our model at low k and ω are much more extended along wave number than along frequency, as reflected in the fact that wave-number spectra have fewer and broader peaks than frequency spectra. Indeed, summing Eq. (40) over wave number at each frequency produces a temporal frequency spectrum with high power at low frequencies, and spectral peaks at the alpha frequency and its resonant frequencies corresponding to beta1, beta2, gamma, etc. Similarly, summing Eq. (40) over frequency at each wave number produces a wave-number spectrum of the same form as P_e, i.e., with a low-k_x plateau and a high-k_x power-law decrease, with the knee between the two behaviors at $\approx 1/r_e$. Figure 5 shows how the spectra in the temporal and spatial domains are linked via the cortical dispersion relation. We see that for low frequencies ($f \lesssim 100$ Hz), the dispersion relation influences the brain dynamics of our model strongly only for $k \lesssim 50$ m^{-1}. These wave numbers include the first of the three power-law decreases in the theoretical wave-number spectrum, Fig. 2. The power-law exponent g in this region indeed varies with frequency, reflecting the dispersion relation, as found using this model to study scalp wave-number spectra [25].

We now turn our attention to whether temporal frequency affects the k spectrum for wave numbers above ≈ 50 m^{-1} by considering frequency-dependent functions in our model. In this wave-number range K_e is featureless for $f \lesssim 100$ Hz apart from a general decreasing trend with increasing wave number. The functions $K_m = 1/|k^2 + q_m^2|$ and $K_i = 1/|k^2 + q_i^2|$ show no strong structures at all, due to their relatively simple mathematical form, a result of the fact that only the long-range excitatory neurons project to the thalamus. Thus their contribution to spectral shape should be independent of temporal frequency. The dendritic filter functions L_a affect only the vertical scaling of the wave-number spectrum and have no effect on its shape. The single remaining consideration is the behavior of the frequency-dependent quantity M. This remains very close to unity over all frequencies for most parameter regimes; however, there exist certain regions of parameter space in which M does not remain constant over frequency. In particular, M varies with frequency for large values of excitatory intracortical gains G_{ee} and G_{mm}, small values of inhibitory intracortical gain G_{ii}, and large values of the dendritic delay parameter α.

In summary, we find that within the experimental frequency range 0 Hz$< f \lesssim 100$ Hz, the spectral shape is greatly affected by cortical dispersion for wave numbers below ≈ 50 m^{-1}, however at larger wave numbers the spectral shape is largely independent of frequency for most realistic parameters. Note that the normalization of the wave-number spectrum does depend on frequency, and at high frequencies spectral power decreases as ω^{-5}, though this is not of concern here since the spectra presented are arbitrarily normalized.

VI. COMPARISON WITH EXPERIMENT

In this section, we compare the predicted wave-number spectra derived from the model with spectra obtained by experiment. We have previously compared the theory with experimental scalp wave-number spectra [25], which showed excellent agreement over the available data range 7 m^{-1} $\lesssim k_x \lesssim 100$ m^{-1}. We now compare the theory with experimental cortical wave-number spectra which span higher wave numbers due to the better resolution on the cortex. There is very little published experimental data due to which the scope for comparison is limited, and thus we concentrate on those aspects of the model which can be supported or refuted by the available data, pending future studies. The 1D projected spectrum is compared with data obtained by Freeman *et al.* [23] from 1D recording arrays in five human subjects. The 2D theoretical spectrum is compared with data obtained by Barrie *et al.* [24] from three areas of rabbit neocortex.

A. 1D human spectrum

Freeman *et al.* [23] recorded human ECoGs from a linear array of 64 electrodes 3.2 cm long placed on the exposed superior temporal gyrus or motor cortex of five volunteers, four of whom were under propofol anesthesia, the other awake. This array gives a wave-number range of 100 m^{-1} $\lesssim k_x \lesssim 6300$ m^{-1}, though the lower portion 100 m$^{-1} \lesssim k_x \lesssim 200$ m^{-1} is not well resolved since it requires implicit extrapolation of the data beyond the length of the array [54]. The portion above 200 m^{-1} is therefore the most reliable.

The results are shown as broken lines in Fig. 6 (dotted lines for the anesthetized subjects and a dashed line for the awake subject), overplotted with a solid line representing the theoretical spectrum produced from parameters that produce model EEGs similar to actual ones seen in anesthetized subjects [30], as given in Table I (the same spectrum shown in Fig. 2). Both theoretical and experimental spectra are integrated over the frequency range $f = 5$–50 Hz. There is no obvious difference between the waking and anesthetized spectra. Note that using the model anesthesia parameters, the kernel K_e has similar dependence on wave number to the eyes-closed case depicted in Fig. 5; however, its structure along the ordinate is quite different: the peak at the 10 Hz alpha frequency is greatly reduced and its harmonic peaks entirely absent, and the strongest structure is at 3 Hz. This mimics the changes in the frequency content of signals recorded from subjects under anesthesia [55,56].

Freeman *et al.* [23] found a low-k_x plateau followed by a monotonic decrease in power with increasing spatial fre-

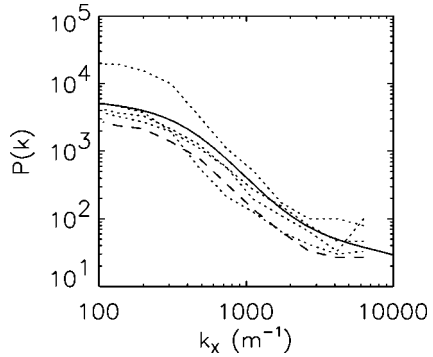

FIG. 6. One-dimensional wave-number power spectrum for human brains under anesthesia, for 5 Hz$\leqslant f \leqslant$50 Hz. The theoretical spectrum derived from the model, using parameters for anesthesia in Table I (solid line), and cortical data recorded by Freeman *et al.* (Ref. [23]) from four subjects under anesthesia (dotted lines) and one awake subject (dashed line).

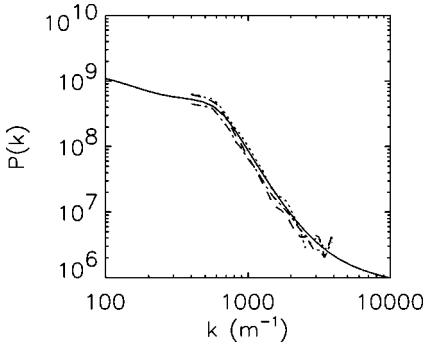

FIG. 7. Two-dimensional wave-number power spectrum for awake rabbit brains, for 5.0 Hz$\leqslant f \leqslant$100 Hz. The anisotropic theoretical spectrum derived from the model, using parameters for rabbits in Table I (solid line), and cortical data recorded by Barrie *et al.* (Ref. [24]) from three neocortical areas (broken lines).

quency up to $\approx$2500 m^{-1}. Above this, the power fluctuated about a baseline, which Freeman *et al.* [23] argued was due to high intensity narrow band noise above 60 Hz. They addressed the appearance of the low-k_x plateau by arguing that the concave-downward nature of the spectrum supports a dipole model of cortical activity with fixed dipole orientation and nonuniform energy distribution, rather than Katznelson's dipole model [57] which assumes uniform energy density and randomly oriented dipoles [13,23]. In the range 250 m$^{-1}\lesssim k_x \lesssim$2500 m^{-1}, Freeman *et al.* [23] measured a power-law exponent $g=1.97\pm0.14$.

Comparing the experimental results with our model's predictions, we see from Fig. 6 that the theoretical curve is in very good agreement with the observed curves. Our model explains the initial plateau and subsequent power-law decrease in terms of filtering through the midrange *m* population in the cortex. The model indicates that rather than representing noise, the high-k_x plateau is likely a real phenomenon occurring as the dominance in cortical activity switches from the midrange excitatory *m* population to the short-scale inhibitory *i* population. For certain parameter regimes, however, such as $r_i \gtrsim 0.5$ mm or $r_m \lesssim 0.5$ mm, our model does not produce the final plateau, so we cannot exclude the possibility that the plateau represents noise; however, these values lie at extremes of the physiologically realistic ranges, as discussed in Sec. IV D. In the range 250 m$^{-1}\lesssim k_x \lesssim$2500 m^{-1} our model produces a power-law spectrum with exponent $g=1.85\pm0.10$ where the uncertainty arises from a slight variation over the frequency range.

Freeman *et al.* [23] extended their analysis to detect possible relations between spatial and temporal spectra by calculating the wave-number spectra in ten bins each 5-Hz wide, up to 50-Hz [23]. The general shape of the spectrum was unchanged over the frequency bins. For the anesthetized subjects, the power-law exponent *g* was not frequency dependent; however, for the awake subject it increased from 1.5 at the alpha frequency ($\approx$10 Hz) to 2.5 at the gamma frequency ($\approx$40 Hz). The theory presented here predicted in Sec. IV B that the spectrum is independent of temporal frequency for $k_x \gtrsim 50$ m^{-1}. This agrees with Freeman's observations for anesthetized subjects, however, does not explain the observed increase in *g* for the awake subject. Increasing the range parameter r_i to 0.5 mm gives a slight frequency-dependent increase in *g* in our model; however, it is not sufficient to explain results of Freeman *et al.* In any case, Freeman *et al.* studied only one awake subject and concluded that this was insufficient to deduce robust differences between waking and sleep spectra, so we leave the resolution of this possible discrepancy for future work.

Neither theoretical nor experimental results provide evidence that *g* fluctuates with frequency at high *k* as it does for $k \lesssim 50$ m^{-1} [19,20,25]. This supports our argument that dispersion related temporal effects do not significantly influence the shape of wave-number spectra at large *k*.

B. 2D rabbit spectrum

Barrie *et al.* [24] implanted square arrays of 64 electrodes with 0.79-mm interelectrode spacing onto the epidural surface of the left hemisphere of rabbit neocortex. Such an array gives data over a wave-number range 400 m$^{-1}\lesssim k \lesssim$4000 m^{-1}, though the portion 400 m$^{-1}\lesssim k \lesssim$700 m^{-1} is not well resolved because it requires extrapolation beyond the length of the array [54].

Note that Barrie *et al.* padded their 8×8 spatial data points with zeros to give 32×32 points, and showed their results over a wave-number range 200 m$^{-1}\lesssim k \lesssim$4000 m^{-1}, where the lower portion 200 m$^{-1}\lesssim k_x \lesssim$400 m^{-1} contained spurious points as a result of the zero padding; we discard these in the present comparisons.

Ten rabbits were implanted with electrodes, two with arrays on the visual cortex, five on the auditory cortex, and three on the somatic cortex, and recordings were made in the waking state. Experimental spectra were obtained by applying a 2D fast Fourier transform, then radially integrating to obtain the spectrum with respect to a single wave-number parameter *k*. Results of Barrie *et al.* are shown in Fig. 7. Note that the power in the visual cortex has been reduced by a factor of 10 to facilitate comparison of the spectral shape with the theory, which is in any case arbitrarily scaled with respect to power. Each broken line represents the average of 40 spatial spectra for one of the three cortical areas. The

theoretical spectrum is shown in Fig. 7 as a solid line, with parameters given in Table I, integrated over the frequency range 5 Hz$\leqslant f \leqslant$100 Hz.

Figure 7 illustrates excellent agreement between the observed and predicted spectra. Both spectra have a low-k plateau with a knee at $k \approx 600$ m^{-1}, followed by a monotonic decrease in power with increasing frequency for 600 m^{-1} $\lesssim k \lesssim$2400 m^{-1}, and both spectra flatten out at $\sim$2400 m^{-1}. In our model, this shape arises naturally as the midrange excitatory signal which dominates at low k is filtered out, and dominance switches to the short-scale inhibitory population. Note that the peak near 4000 m^{-1} in the experimental data is an artifact reflecting the spatial Nyquist frequency for the electrode arrays [24].

VII. SUMMARY AND DISCUSSION

We have extended our existing continuum model of corticothalamic dynamics by further considering the structures in the brain which can contribute to spatial filtering and hence be important in determining the form of the wave-number power spectrum. The resulting introduction of a short-scale population of excitatory neurons models the excitatory recurrent collateral system.

The model was used to derive the cortical wave-number spectrum. This was found to consist of a low-k_x plateau followed by three regions of power-law decrease, each separated by an incompletely formed plateau. The low-k_x plateau is due to the long-range excitatory e neurons, which dominate at global (low-k_x) scales because of their prevalence, structure, and aligned orientation. The first power-law decrease is due to filtering through these long-range axons, and dominance switches to the midrange m population, giving the second plateau. At larger k_x, the signal is filtered through the midrange axons and dominance switches finally to the inhibitory i population, which is in turn filtered out at very small scales (large k_x). Thus the three power-law regions reflect the filtering through physical structures in the brain, namely, the long-range excitatory axons, the midrange excitatory recurrent collaterals, and the short-range inhibitory axons. The inclusion of any additional neuron populations, such as a short-range excitatory population, would most likely result in an additional region of power-law filtering; however, since the continuum model is not valid at very large k_x and experimental data at very large k_x would require unfeasibly small electrode spacings, the single inhibitory population already included in the theory should suffice to model all populations below $\approx$0.3 mm.

We can view the spectrum as having three distinct wave-number regions, each comprising a power-law region and surrounding plateaus. The first region, ≈ 10 m$^{-1} \lesssim k_x \lesssim 100$ m^{-1}, has been studied previously [25] and shown to give excellent agreement between theory and experimental scalp data, for both eyes-closed and eyes-open conditions. Here we have explored the second wave-number region, 100 m$^{-1} \lesssim k_x \lesssim$6000 m^{-1}, and found extremely good agreement between theory and experiment, using cortical data rather than scalp data because of the finer spatial resolution. With reference to the 1D human data, Freeman *et al.* suggested that the spatial spectrum and its power-law exponent are mainly determined by the depth within the cortex of the current generating neuron, the location of the synapses, and the properties of the dendrites [13,23,58]. In the context of our model, the physiological factors outlined by Freeman *et al.* [13,23,58] indeed affect spectral shape and slope, primarily by their influence on model parameters r_m, W_a, and α. Experimental investigation of the third region, $k_x \gtrsim 6000$ m^{-1}, would require using a cortical array with electrode spacing smaller than 0.5 mm.

We also explored potential relations between temporal and spatial spectra. Within the context of our model there is strong evidence for a cortical dispersion relation, the fine structure of which produces such phenomena as the alpha rhythm and other resonances in the temporal frequency spectrum, and also produces the plateau-plus-power-law form of the wave-number spectrum. In this way the link between the temporal and spatial domains can be easily visualized. Our model predicts that for usual experimental frequencies $f \leqslant 100$ Hz, the wave-number spectrum is strongly dependent on frequency for $k_x \lesssim 50$ m^{-1}, and independent of frequency for $k_x \gtrsim 50$ m^{-1}. Thus, we expect the first wave-number region to reflect the fine structure of the dispersion relation, but the second and third regions to be approximately invariant over frequency. Indeed, we have shown previously [25] that the first region depends strongly on frequency via fluctuation of the power-law exponent g over frequency. We have shown here that the exponent g and spectral shape in the second region do not depend on frequency.

Similarly, Freeman *et al.* [23] found no evidence for dispersion related effects for the anesthetized patients over the wave-number range they investigated, 250 m$^{-1} < k_x < 2500$ m^{-1}, in agreement with our model. For the single waking subject, however, Freeman *et al.* found an increase in the power-law exponent g with increasing temporal frequency, contrary to our prediction that the wave-number spectrum is independent of frequency in this wave-number region. More experiments are needed to determine whether this represents a robust difference between anesthetized and waking spectra.

The 2D spectrum was also derived here and compared with experiment. We have shown that in the 2D cortical spectrum, the magnitude of the maximum theoretical power-law exponent g is 4. In the 1D projected cortical spectrum, the maximum exponent decreases to 3 due to the integration over one dimension in k space. We have shown previously [25] that for scalp spectra the maximum exponent increases due to additional filtering through the head.

The theoretical 2D spectrum was presented for parameters corresponding to a rabbit cortex by scaling the relevant human parameters to account for known differences between human and rabbit physiology. A possible concern is that boundary conditions would have a greater influence on dynamics in the smaller rabbit brain, however, the corresponding increase in long-range cortical damping would mitigate the effects. In any case, possible effects would be significant only at large scales, not at the relatively large wave numbers studied here. Thus there is conceivably very little influence from boundary conditions in the rabbit brain, which is fur-

ther supported by the excellent agreement between the infinite 2D model and the experimental results obtained by Barrie *et al.* [24].

The analysis of wave-number power spectra using this theory enables us to noninvasively probe physiology and to estimate parameters such as mean neuronal range. Another technique which enables noninvasive probing of physiology and brain state is the calculation of correlation and coherence functions. These quantities have been previously studied using our model [31], and comparison with data pointed to the existence of an excitatory neuron population with mean range ≈ 6 mm. This range is consistent with the midrange population introduced here, further supporting the assertion that such a population significantly affects cortical dynamics.

In conclusion, we have extended our existing model of corticothalamic dynamics to investigate the wave-number power spectrum on the cortical surface. Both the two-dimensional spectrum and its projection into one dimension have been explored, and shown to agree with experiment. Spectral features such as plateaus arise naturally in our model, in agreement with experiment, whereas previously such features have typically been viewed as aberrant. We have presented evidence of a cortical dispersion relation and discussed the wave-number and frequency ranges within which it is expected to significantly influence dynamics. The spatial analysis presented represents one facet of a model which is able to reproduce many apparently disparate aspects of brain behavior in a unified way.

Full exploration and verification of the theory would require more wave-number data than are presently available. Furthermore, with sufficient data, the predicted spectra could be fitted in detail to the observed spectra in order to provide insight into the parameters' values from a new perspective. Similarly, direct physiological measurements of inferred parameters would explicitly test their accuracy. Thus, more *k*-space experiments, covering larger ranges of wave numbers, would also enable further comparisons with the theory, thereby strengthening confidence in its predictions.

ACKNOWLEDGMENTS

The authors thank C. J. Rennie, D. L. Rowe, and M. Breakspear for stimulating discussions and valuable comments. This work was supported by a University of Sydney Sesqui Grant.

[1] M.C. Steriade, D.A. McCormick, and T.J. Sejnowski, Science **262**, 679 (1993).
[2] R.R. Llinás and D. Paré, Neuroscience **44**, 521 (1991).
[3] M. Schoppenhorst, F. Brauer, G. Freund, and St. Kubicki, Electroencephalogr. Clin. Neurophysiol. **48**, 25 (1980).
[4] E. Niedermeyer, Int. J. Psychophysiol **26**, 31 (1997).
[5] F. Aoki, E.E. Fetz, L. Shupe, E. Lettich, and G.A. Opejman, Clin. Neurophys. **110**, 524 (1999).
[6] A.W. de Weerd, W.V.M. Perquin, and E.J. Jonkman, Dementia **1**, 115 (1990).
[7] M.Y. Neufeld, S. Blumen, I. Aitkin, Y. Parmet, and A.D. Korczyn, Dementia **5**, 23 (1994).
[8] A. Stevens and T. Kircher, Eur. Arch. Psychiatry Clin. Neurosci. **248**, 259 (1998).
[9] H. Tanaka, T. Koenig, R.D. Pascual-Marqui, K. Hirata, K. Kochi, and D. Lehmann, Dement Geriatr. Cogn. Disord. **11**, 39 (2000).
[10] L. Pezard, R. Jech, and E. Ružička, Clin. Neurophysiol. **112**, 38 (2001).
[11] W.J. Freeman, Electroencephalogr. Clin. Neurophysiol. **44**, 586 (1978).
[12] W.J. Freeman and W. Schneider, Psychophysiology **19**, 44 (1982).
[13] W.J. Freeman and B.W. van Dijk, Brain Res. **422**, 267 (1987).
[14] N.E. Crone, D.L. Miglioretti, B. Gordon, J.M. Sieracki, M.T. Wilson, S. Uematsu, and R.P. Lesser, Brain **121**, 2271 (1998).
[15] V. Menon, W. Freeman, B.A. Cutillo, J.E. Desmond, M.F. Ward, S.L. Bressler, K.D. Laxer, N. Barbaro, and A.S. Gevins, Electroencephalogr. Clin. Neurophysiol. **98**, 89 (1996).
[16] P.L. Nunez, B.M. Wingeier, and R.B. Silberstein, Human Brain Mapp. **13**, 125 (2001).
[17] E. Niedermeyer and F.H. Lopes da Silva, *Electroencephalography: Basic Principles, Clinical Applications, and Related Fields*, 4th ed. (Williams and Wilkins, Baltimore, 1999).
[18] B. Shen, M. Nadkarni, and R.A. Zappulla, Clin. Neurophys. **110**, 115 (1999).
[19] G.R. Shaw, *Spherical Harmonic Analysis of the Electroencephalogram*, Ph.D. dissertation, University of Alberta, Alberta, Canada, 1991 (unpublished).
[20] B.M. Wingeier, P.L. Nunez, and R.B. Silberstein, Phys. Rev. E **64**, 051916 (2001).
[21] P.L. Nunez, *Neocortical Dynamics and Human EEG Rhythms* (Oxford, New York, 1995).
[22] W.J. Freeman and B. Baird, Behav. Neurosci. **101**, 393 (1987).
[23] W.J. Freeman, L.J. Rogers, M.D. Holmes, and D.L. Silbergeld, J. Neurosci. Methods **95**, 111 (2000).
[24] J.M. Barrie, W.J. Freeman, and M.D. Lenhart, J. Neurosci. **16**, 520 (1996).
[25] S.C. O'Connor, P.A. Robinson, and A.K.I. Chiang, Phys. Rev. E **66**, 061905 (2002).
[26] P.A. Robinson, J.J. Wright, and C.J. Rennie, Phys. Rev. E **57**, 4578 (1998).
[27] P.A. Robinson, P.N. Loxley, S.C. O'Connor, and C.J. Rennie, Phys. Rev. E **63**, 041909 (2001).
[28] C.J. Rennie, P.A. Robinson, and J.J. Wright, Biol. Cybern. **86**, 457 (2002).
[29] P.A. Robinson, C.J. Rennie, J.J. Wright, H. Bahramali, E. Gordon, and D.L. Rowe, Phys. Rev. E **63**, 021903 (2001).
[30] P.A. Robinson, C.J. Rennie, and D.L. Rowe, Phys. Rev. E **65**, 041924 (2002).
[31] P.A. Robinson, J. Theor. Biol. (to be published).
[32] D.L. Rowe, P.A. Robinson, C.J. Rennie, and R.C. Powles (unpublished).
[33] L.J. Pinson and D.G. Childers, IEEE Trans. Biomed. Eng. **21**, 3 (1974).

[34] P.L. Nunez, IEEE Trans. Biomed. Eng. **21**, 473 (1974).
[35] P.L. Nunez, Math. Biosci. **21**, 279 (1974).
[36] J.J. Wright and R.R. Kydd, Biol. Cybern. **50**, 89 (1984).
[37] W.M. Kistler, R. Seitz, and J.L. Van Hemmer, Physica D **114**, 273 (1998).
[38] F.H. Lopes da Silva, A. Hoeks, H. Smits, and L.H. Zetterberg, Kybernetik **15**, 27 (1974).
[39] M.C. Steriade, P. Gloor, R.R. Llinás, F.H. Lopes da Silva, and M.M. Mesulam, Electroencephalogr. Clin. Neurophysiol. **76**, 481 (1990).
[40] W.J. Freeman, Int. J. Bifurcation Chaos Appl. Sci. Eng. **2**, 451 (1992).
[41] J.J. Wright and D.T.J. Liley, Behav. Brain Sci. **19**, 285 (1996).
[42] P.A. Robinson, C.J. Rennie, and J.J. Wright, Phys. Rev. E **56**, 826 (1997).
[43] E.G. Jones, *The Thalamus* (Plenum, New York, 1985).
[44] W. Rall, J. Neurophysiol. **30**, 1138 (1967).
[45] J. DeFelipe, M. Conley, and E.G. Jones, J. Neurosci. **6**, 3749 (1986).
[46] J. DeFelipe and E.G. Jones, *Cajal on the Cerebral Cortex* (Oxford, New York, 1988).
[47] M.S. Cynader, J. Neurosci. **7**, 1401 (1987).
[48] A. Grinvald, J. Neurosci. **14**, 2545 (1994).
[49] E.T. Rolls and A. Treves, *Neural Networks and Brain Function* (Oxford, New York, 1991).
[50] V. Braitenberg and A. Schuz, *Anatomy of the Cortex. Statistics and Geometry* (Springer-Verlag, New York, 1991).
[51] H.A. Swadlow, J. Neurophysiol. **63**, 1477 (1990).
[52] H.A. Swadlow, J. Neurophysiol. **66**, 1392 (1991).
[53] R.D. Katznelson, in *Electric Fields of the Brain: The Neurophysics of EEG*, edited by P.L. Nunez (Oxford, New York, 1981).
[54] P.L. Nunez, *Electric Fields of the Brain: The Neurophysics of EEG* (Oxford, New York, 1981).
[55] N.T. Smith, H. Dec-Silver, T.J. Sanford, Jr., C.J. Westover, Jr., M.L. Quinn, F. Klein, and D.A. Davis, Anesth. Analg. (Paris) **63**, 386 (1984).
[56] M. Ghignone, L. Quintin, P.C. Duke, C.J. Kehler, and O. Calvillo, Anesthesiology **64**, 36 (1986).
[57] R.D. Katznelson, doctoral dissertation, University of California, San Diego, 1982 (unpublished).
[58] W.J. Freeman, *Mass Action in the Nervous System* (Academic Press, New York, 1975).